Proceedings of the ASME 2019
International Design Engineering Technical Conferences
and Computers and Information in Engineering Conference
IDETC/CIE2019
August 18-21, 2019, Anaheim, CA, USA

IDETC2019/MESA-12345

DRAFT: ENERGETICALLY-OPTIMAL DISCRETE AND CONTINUOUS STABILIZATION OF THE RIMLESS WHEEL WITH TORSO

Wankun Sirichotiyakul, Aykut C. Satici
Dept. of Mechanical and Biomedical Engineering
Boise State University
Boise, Idaho 83725
Email: {wankunsirichotiyakul, aykutsatici}@boisestate.edu

Sebastian Sanchez, Pranav A. Bhounsule *
Dept. of Mechanical Engineering
University of Texas San Antonio
San Antonio, Texas 78249
Email: {eric.sanchez3, pranav.bhounsule}@utsa.edu

ABSTRACT

In this work, we discuss the modeling, control, and implementation of a rimless wheel with torso. We derive and compare two control methodologies: a discrete-time controller (DT) that updates the controls once-per-step and a continuous-time controller (CT) that updates gains continuously. For the discrete controller, we use least-squares estimation method to approximate the Poincaré map on a certain section and use discrete-linear-quadratic-regulator (DQLR) to stabilize a (closed-form) linearization of this map. For the continuous controller, we introduce moving Poincaré sections and stabilize the transverse dynamics along these moving sections. For both controllers, we estimate the region of attraction of the closed-loop system using sum-of-squares methods. Analysis of the impact map yields a refinement of the controller that stabilizes a steady-state walking gait with minimal energy loss. We present both simulation and experimental results that support the validity of the proposed approaches. We find that the CT controller has a larger region of attraction and smoother stabilization as compared with the DT controller.

*The NSF grant 1816925 supported the work done by SS and PAB.

1 Introduction

Passive dynamic legged robots attain locomotion solely through gravitational potential energy. Perhaps the simplest and most popular of its kind is a multi-spoked wheel with the rim removed, first developed by McGeer [1] almost two decades ago. When a rimless wheel is launched downhill at a slope of angle γ with respect to the horizontal, it is able to sustain steady locomotion as the kinetic energy lost through spoke impacts is supplied back to the system by the potential energy of traveling downhill. As a result, these robots are highly energy efficient because no external energy needs to be provided for stabilization. However, unless actuated in some way, there are two major limitations of passive dynamic robots: (1) they cannot sustain dynamically stable walking uphill or on level ground [2], and (2) they are not robust to external disturbances.

One way to enable sustained locomotion of a rimless wheel on level ground is to have a design that incurs zero kinetic energy losses during impacts, which is achievable by reducing the spoke collision velocity to zero. Gomes [3] uses an inertial disk that is coupled to the rimless wheel through a torsional spring, thus storing and releasing energy to the robot at appropriate times. Such a robot will need a shallow ramp to sustain walking motion in reality to compensate for the dissipation in the springs, inertia disk, and frictional losses.

Another way to enable walking is to have an actively pow-

ered rimless wheel. Some extensions to the rimless wheel of this sort can be found in [4,5] where the spokes expand and contract, thus supplying energy to the robot. A drawback of this implementation is that it requires multiple actuators. Other examples include rimless wheels with a wobbling mass [6] or a rotating disc [7] that transfers energy through dynamic coupling.

Bhounsule [8] designed a rimless wheel with a torso which may be actuated to provide the necessary kinetic energy for continuous walking on level or uphill slopes. The torso position is regulated at a certain moment during the gait by an event-based, discrete controller. This controller assumes the unrealistic ability to instantaneously change the torso angle. We show in the paper that there are performance benefits of continuously moving the torso including energy efficiency and robustness.

The rimless wheel with torso is modeled as a hybrid dynamical system, that exhibits both continuous and discrete phases [9, 10]. A common approach to study the periodic stability of such systems involves an analysis of the Poincaré map. Local orbital stability is characterized by the stability of an associated "first-return map" that describes the repeated, discrete passes of the system through a single, predefined transversal hypersurface.

In this work, we provide novel results in the design, analysis, and implementation of discrete- and continuous-time controllers. The contributions of this paper are summarized below:

- Design two novel controllers for a reduced system,
- Estimate and compare the regions of attractions of these controllers,
- Provide an implementation of these controllers on the full system dynamics that guarantee its stability,
- Provide an analysis of the impact map that yields an optimization procedure to find energetically-preferable nominal walking gaits,
- Provide extensive simulation and partial experimental support for the theory.

2 System Model

The robot consists of two parts, first of which is the classical rimless wheel and the second of which is a torso attached to the rimless wheel at its center. The rimless wheel consists of $n = 10$ massless spokes, each of length l_1. The rimless wheel has mass m_1, which is concentrated at the hip. A point mass m_2 is attached to the hip through a massless rod of length l_2 and constitutes the torso. We place a motor between the torso and the hip and actuate the variable φ, defined as the angle between the normal vector that penetrates the terrain and the vector that emanates from the hip and is directed to the point mass m_2. The position of the hip is characterized by the angle θ, which is defined between the normal vector that penetrates the terrain and the vector that emanates from the hip and is directed to the point of contact. A downhill terrain is characterized by a ramp slope, $\gamma > 0$. Without loss of generality, we assume that the wheel walks from left-to-right, that is, for walking we must have $\dot{\theta}(t) < 0$ for all $t > 0$. Finally, we denote half the angle between two spokes by $\alpha = \frac{\pi}{n}$. This system is depicted in Figure 1 along with the definitions of important parameters and variables.

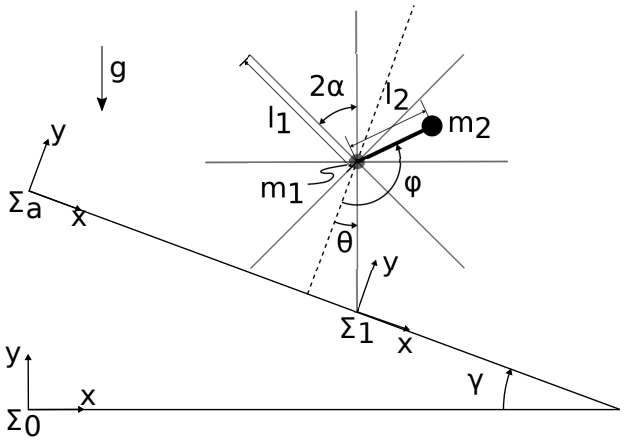

FIGURE 1: Rimless wheel with torso depicted with $n = 8$ spokes. The angle φ is controlled.

Rimless wheel is a system that undergoes phases of continuous flows and discrete transitions, resulting in a hybrid dynamical system with two modes. Its configuration space is $\mathscr{Q} = \mathbb{T}^2$, the two-torus. The state space is then the tangent bundle of the configuration space, denoted by $T\mathscr{Q}$.

2.1 Swing model – continuous dynamics

We derive the continuous dynamics of the system via the Lagrangian approach. The kinetic and potential energies of the system are given by

$$\mathscr{K} = \frac{1}{2}\sum_{i=1}^{2} m_i v_i \cdot v_i + \frac{1}{2}\sum_{i=1}^{2} \omega_i \cdot I_i \omega_i,$$
$$\mathscr{P} = \sum_{i=1}^{2} m_i g\, p_{0,i} \cdot e_2,$$

where $\{v_i\}_1^2$ are the linear velocities of the hip, and the tip of the torso; $\{\omega_i\}_1^2$ are the angular velocities of the wheel and the torso with respect to and expressed in the inertial frame; $\{p_{0,i}\}_1^2$ are the position vectors from the origin of the inertial frame to the centers of mass of the wheel and the torso, $\{m_i\}_1^2$ and $\{I_i\}_1^2$ are masses and the moments of inertia of the wheel and the torso about their centers of masses, respectively. The magnitude of the gravitational acceleration is denoted by g while its opposite direction is given by $-e_2$. In coordinates (θ, φ) (see Figure 1), the Lagrangian is given by

$$\begin{aligned}\mathscr{L} &= \mathscr{K} - \mathscr{P} \\ &= \frac{1}{2}\left(I_1 + m_t l_1^2\right)\dot{\theta}^2 - m_2 l_1 l_2 c_{\theta\varphi}\dot{\theta}\dot{\varphi} \\ &\quad + \frac{1}{2}\left(I_2 + m_2 l_2^2\right)\dot{\varphi}^2 - m_t g l_1 c_{\theta\gamma} + m_2 g l_2 c_{\varphi\gamma},\end{aligned}$$

where $m_t = m_1 + m_2$, $c_{ab} := \cos(a-b)$ and $s_{ab} := \sin(a-b)$, with a and b taking values in $\{\theta, \varphi, \gamma\}$. Defining $q = (\theta, \varphi)$ and writing the Euler-Lagrange equations corresponding to this Lagrangian yields the classical robot dynamics

$$M(q)\ddot{q} + C(q,\dot{q})\dot{q} + G(q) = Bu, \tag{1}$$

where $B = \begin{bmatrix}-1 & 1\end{bmatrix}^\top$ and

$$\begin{aligned}M(q) &= \begin{bmatrix} I_1 + m_t l_1^2 & -m_2 l_1 l_2 c_{\theta\varphi} \\ -m_2 l_1 l_2 c_{\theta\varphi} & I_2 + m_2 l_2^2 \end{bmatrix}, \\ C(q,\dot{q}) &= m_2 l_1 l_2 s_{\theta\varphi}\begin{bmatrix} 0 & -\dot{\varphi} \\ \dot{\theta} & 0 \end{bmatrix}, \\ G(q) &= g\begin{bmatrix} -m_t l_1 s_{\theta\gamma} \\ m_2 l_2 s_{\varphi\gamma}\end{bmatrix},\end{aligned}$$

Adding the two and setting $\dot{\varphi} \equiv 0$ in this equation yields what we will call the *reduced equations of motion*.

$$\tilde{m}(q)\ddot{\theta} + \tilde{c}(q,\dot{\theta})\dot{\theta} + \tilde{g}(q) = 0, \tag{2}$$

where

$$\begin{aligned}\tilde{m}(q) &= I_1 + m_t l_1^2 - m_2 l_1 l_2 c_{\theta\varphi}, \\ \tilde{c}(q,\dot{\theta}) &= m_2 l_1 l_2 s_{\theta\varphi}\dot{\theta}, \\ \tilde{g}(q) &= -m_t g l_1 s_{\theta\gamma} + m_2 g l_2 s_{\varphi\gamma}.\end{aligned}$$

This reduced model, with configuration space $\mathscr{Q} = \mathbb{S}^1$, where $\mathbb{S}^1$ stands for the circle as a topological space, neglects the transient response of the torso, whose angle φ is viewed as the control input.

2.2 Impact model – discrete transition

At heelstrike, the impulsive reaction force from the ground is applied at the end of the swing leg. The angular momentum of the whole system about the swing foot is not affected by this reaction force [11], implying a conservation law relating the pre-impact and post-impact velocities of the system. Similarly, the impact force affects the torso through the hip. Therefore, the angular momentum of the torso about this point is conserved through the heelstrike. Combining these two observations yields the impact map for the system. Representing the state of the system in coordinates by $x := (q,\dot{q}) = (\theta, \varphi, \dot{\theta}, \dot{\varphi})$, the impact map, $\Delta : T\mathscr{Q} \to T\mathscr{Q}$, is given by

$$x^+ = \Delta(x^-) = \Xi(q)x^-, \tag{3}$$

where $\mathbb{R}^{4\times 4} \ni \Xi(q) = \mathrm{diag}\{\Xi_p, \Xi_v\}$ has a block diagonal structure with $\Xi_p = \mathrm{diag}\{-1, 1\}$ and

$$\begin{aligned}\Xi_v(q) &= \begin{bmatrix}\xi_1(\varphi) & 0 \\ \xi_2(\varphi) & 1\end{bmatrix}, \\ \left|\Xi_v^+\right| &= I_1 I_2 + I_1 m_2 l_2^2 + I_2 m_t l_1^2 \\ &\quad + m_2 l_1^2 l_2^2\left(m_1 + m_2\sin(\alpha-\varphi)^2\right), \\ \left|\Xi_v^+\right|\xi_1(\varphi) &= I_1 I_2 + I_1 m_2 l_2^2 \\ &\quad + \left[I_2 m_t l_1^2 + m_2 l_1^2 l_2^2\left(m_1 + \frac{m_2}{2}\right)\right]\cos(2\alpha) \\ &\quad - \frac{1}{2}m_2^2 l_1^2 l_2^2\cos(2\varphi), \\ \left|\Xi_v^+\right|\xi_2(\varphi) &= m_2 l_1 l_2\left[I_1\left(\cos(\alpha-\varphi) - \cos(\alpha+\varphi)\right)\right. \\ &\quad \left. + m_t l_1^2\left(\cos(2\alpha)\cos(\alpha-\varphi) - \cos(\alpha+\varphi)\right)\right].\end{aligned}$$

For the reduced model, we again set $\dot{\varphi} \equiv 0$, which reduces these equation to yield the *reduced impact map*, $\Xi_r(q) = \mathrm{diag}\{-1, \xi_r(q)\}$, where

$$\begin{bmatrix}\theta^+ \\ \dot{\theta}^+\end{bmatrix} = \Xi_r(q)\begin{bmatrix}\theta^- \\ \dot{\theta}^-\end{bmatrix}, \tag{4a}$$

$$\xi_r(q) = \frac{I_1 + m_t l_1^2\cos(2\alpha) - m_2 l_1 l_2\cos(\alpha+\varphi)}{I_1 + m_t l_1^2 - m_2 l_1 l_2\cos(\alpha-\varphi)}. \tag{4b}$$

2.3 Hybrid model

The overall model of walking is obtained by combining the swing phase model and the impact model to form a system with impulse effects. For the full model with $x = (q,\dot{q})$, we have

$$\Sigma : \begin{cases}\dot{x} = f(x,u) & \text{if } x^- \notin \mathscr{S} \\ x^+ = \Delta(x^-) & \text{if } x^- \in \mathscr{S},\end{cases} \tag{5}$$

where the switching set is chosen to be

$$\mathscr{S} := \left\{x \in T\mathscr{Q} : p_2^v(\theta) = 0, p_2^h(\theta) > 0\right\}.$$

Here p_2^h and p_2^v denote the x- and y- position of the swing leg with respect to the auxiliary frame, Σ_a, (see Figure 1). In the equations

of motion (5), the flow vector field f is taken from equation (1). The impact map is given by $\Delta(x) = \Xi(q)x$.

For a preliminary controller design, it will be convenient to use the reduced model, where we view the torso angle φ as the control input and reduce the states to $x = (\theta, \dot{\theta})$. In this case, the flow vector field in (5) is taken from equation (2) and the reduced impact map is given by $\Delta(x) = \Xi_r(q)x$.

3 Control Design

In this section, we present two novel controllers, an inherently discrete-time and an inherently continuous-time, derived from the reduced model and stabilized on the full system. We describe how to estimate the regions of attraction of these controllers and present an analysis that leads to further performance improvements. An overview of the control design procedure is given in Algorithm 1.

3.1 Discrete-Time (DT) Controller

For this type of controller, we seek to set the torso angle at a particular Poincaré section that we choose to be $\mathscr{S} = \{x \in \mathbb{S}^1 \times \mathbb{R} : \theta = 0\}$. The torso angle is then kept constant throughout the swing phase.

The set polynomial functions forms a basis for the space of continuous functions from $\mathbb{R}$ to $\mathbb{R}$. We use this fact to approximate the Poincaré map by a polynomial of the form

$$P(y,u) = \sum_{\eta_1+\eta_2 \leq m} \alpha_\eta y^{\eta_1} u^{\eta_2}, \tag{6}$$

where $\eta = (\eta_1, \eta_2)$ is a multi-index, that is, a 2-tuple of non-negative integers, whose sum is less than or equal to m, the degree of the approximating polynomial. Note that $P : U \subseteq \mathscr{S} \to \mathscr{S}$ is a map from a subset of the Poincaré section to the Poincaré section. Here $y = \dot{\theta} - \dot{\theta}^\star$ is the coordinate along the Poincaré section with $\dot{\theta}^\star$ denoting the nominal wheel velocity along a nominal walking gait, and u is the torso angle, φ.

We invoke the least squares estimation technique to estimate the coefficients, $\{\alpha_\eta\}$, of this polynomial. The estimation is performed by generating target values, $\dot{\theta}_{\text{target}}$ on the Poincaré section, by simulating forward in time a range of initial values $0 < \dot{\theta} < -\pi$ and $\gamma < \varphi < \frac{\pi}{2} + \gamma$. We remove from data the failed simulations due to stumbling or running. These target values are then compared with the output of the approximation of the Poincaré map and the coefficients that minimize the discrepancy are selected. In other words, $\{\alpha_\eta\}$ are found by solving the following minimization problem

$$\underset{\alpha_\eta}{\text{minimize}} \quad \|P(\dot{\theta}, \varphi) - \dot{\theta}_{\text{target}}\|^2.$$

We use a linear approximation to derive the discrete-time controller and test the controller against a second-order approximation to avoid potential overfitting. This linear approximation of the Poincaré map allows for the use of the mature theory of linear systems and we choose to utilize a DLQR controller for the discrete linear system

$$y_{k+1} = P(y_k, u_k) = \alpha_{1,0} y_k + \alpha_{0,1} u_k. \tag{7}$$

3.2 Continuous-Time (CT) Controller

We use the method described in [12, 13] to derive a continuous-time (CT) controller for the reduced system. In this case, instead of sticking to a particular Poincaré section, we choose a family of Poincaré sections, one for each parameter $\tau \in \mathbb{R}$, along a periodic orbit of the system. As θ is a monotonically decreasing function of time along a periodic orbit, we use this state variable to parametrize the Poincaré sections, i.e. $t = \tau(\theta)$, where t denotes the time. Using this parametrization, we have the following family of Poincaré sections

$$\mathscr{S}(\theta) = \{x \in \mathbb{S}^1 \times \mathbb{R} : \theta = c, \text{ for some } c \in [-\alpha, \alpha]\}.$$

This family of Poincaré sections can also be described as a family of hyperplanes defined as follows

$$\mathscr{S}(\theta) = \left\{y \in \mathbb{R}^2 : z^\top (y - x^\star(\theta)) = 0\right\},$$

where $z = \begin{bmatrix}-1 & 0\end{bmatrix}^\top$ and $x^\star(\theta)$ is a periodic orbit, i.e., $x^\star(t) = x^\star(t+T)$ with $\dot{x}^\star(t) \neq 0, \forall t \in [0, T)$. We construct a coordinate system on $\mathscr{S}(\theta)$ by choosing the basis on this subspace as $\begin{bmatrix}0 & -1\end{bmatrix}^\top$. A projection operator $\Pi(\theta)$ onto this space is then defined as $\Pi(\theta) = \begin{bmatrix}0 & 1\end{bmatrix}$. This construction defines a change of coordinates $x \mapsto (x_\perp, \tau)$, where τ represents which of the transversal surfaces $\mathscr{S}(\tau)$ the current state x inhabits, and the vector $x_\perp$ is the "transversal" state representing the location of x within the hyperplane $\mathscr{S}(\tau)$, with $x_\perp = 0$ implying that $x = x^\star(\tau)$. The transverse coordinate under this construction is determined by $x_\perp = \Pi(y - x^\star(\tau))$ for any $y \in \mathscr{S}(\tau)$.

The transverse dynamics for the rimless wheel with torso is given by

$$\dot{x}_\perp = \Pi f\left(x^\star(\tau) + \Pi^\top x_\perp\right) - \Pi f(x^\star(\tau))\,\dot{\tau}, \tag{8a}$$

$$\dot{\tau} = \frac{z^\top f\left(x^\star(\tau) + \Pi^\top x_\perp\right)}{z^\top f(x^\star(\tau))}. \tag{8b}$$

In order to derive a CT controller, we compute the linearization of the transverse dynamics (8).

$$\dot{\delta x}_\perp = a(t)\delta x_\perp + b(t)\delta u, \tag{9}$$

where

$$a(t) = \Pi \frac{\partial f}{\partial x}(x^\star(t))\Pi^\top - \Pi f(x^\star(t)) \left.\frac{\partial \dot{\tau}}{\partial x_\perp}\right|_{x_\perp=0}, \tag{10a}$$

$$b(t) = \Pi \frac{\partial f}{\partial u}(x^\star, u^\star). \tag{10b}$$

For evaluating the right-hand sides of these expressions, first we stabilize a limit cycle using the methods discussed in Section 3.5. The limit cycle thus provided is then interpolated to be a function of time and are inserted into equation (10).

We follow this procedure up by solving the differential Riccati equation corresponding to this linear time-varying (LTV) system and come up with an optimal gain such that $\delta u(t) = k(t)\delta x_\perp(t)$. We apply this feedback control as a function of the phase variable θ rather than time t, by setting $k(t) = k \circ \tau(\theta)$. This renders the overall closed-loop system autonomous rather than time-varying, which simplifies further stability analyses.

Algorithm 1: Controller Design Process

Input: States of the robot in the reduced model, $x = (\theta, \dot{\theta})$
Output: Desired torso angles φ_{ref}, stabilizing a nominal walking gait of the reduced model

```
x* ← Find a nominal limit cycle
if Discrete-time controller then do
    Define a single Poincaré section along x*
    P ← approximation of the Poincaré map
    Design a DLQR controller to stabilize the fixed point of P
    φ_ref ← φ_0 + K(θ̇ − θ̇*)
else if Continuous-time controller then do
    Define a family of Poincaré sections along x*, each
      parametrized by τ
    Define a transverse coordinate x_⊥
    Transform original coordinates to (τ, x_⊥) coordinates
    Compute the nonlinear dynamics of the transverse system
    Linearize the transverse dynamics
    Design a LQR controller to stabilize the x_⊥ system
    φ_ref ← φ_0 + k(θ)(θ̇ − θ̇*)
return φ_ref
```

3.3 Implementation of the Controllers

Both of the controllers we have derived so far find desired torso angles, which would stabilize a nominal walking gait for the reduced model. The DT controller yields an angle to be kept constant for each step, whereas the CT controller yields a time-varying, continuous reference torso angle. We will call both reference signals φ_{ref} henceforth.

In this short subsection, we describe how to make the torso angle φ exponentially track φ_{ref}. For this purpose, we employ the now-standard method of partial feedback linearization [14] on the equations (1). We solve the first equation in (1) for $\ddot{\theta}$ and substitute it into the second to get the following equation

$$\begin{aligned}\Delta_{22}\ddot{\varphi} + h(q,\dot{q}) &= bu,\\ h(q,\dot{q}) &= c_{21}\dot{\theta} - m_{12}^\top m_{11}^{-1} c_{12}\dot{\varphi} + g_2 - m_{12}^\top m_{11}^{-1} g_1,\end{aligned}$$

where Δ_{22} is the Schur complement of the block m_{22} of the matrix M, and $b = 1 + m_{12}^\top m_{11}^{-1}$. Expanding the expression for b, one finds out that it vanishes nowhere. Thus, we can set

$$u = \frac{1}{b}\left(h - \Delta_{22}\left(k_p(\varphi - \varphi_{ref}) + k_d(\dot{\varphi} - \dot{\varphi}_{ref})\right)\right), \tag{11}$$

which is well-defined on all of the state-space. Here k_p and k_d are positive control gains. Since $\varphi_{ref} = \varphi_0 + k(\theta)(\dot{\theta} - \dot{\theta}^\star)$, this implies on the nominal limit cycle, $\varphi = \varphi_0$. Combined with Proposition 2, this implies that the perturbation to the reduced dynamics of the motion of the torso is a vanishing perturbation that is Lipschitz in a neighborhood of $x_\perp = 0$. Thus by Lemma 9.1 of [15], this implies that the full system is locally exponentially stable to the nominal limit cycle.

3.4 Region of Attraction Estimation

We have devised two controllers for the rimless wheel with torso. Both of these controllers are derived from the linearization of a relevant dynamical quantity. It is then of interest to quantify the regions of attraction of these controllers. We solve this estimation problem by casting it as the following sum-of-squares program.

$$\begin{aligned}\text{maximize} \quad & \rho\\ \text{subject to} \quad & (V(y) - \rho) - \lambda(y)\,\mathrm{d}V(y) \text{ is SOS},\\ & \lambda(y) \text{ is SOS},\end{aligned} \tag{12}$$

where $y = \dot{\theta} - \dot{\theta}^\star$ and the term SOS implies a sum-of-squares constraint [16]. We pick the Lyapunov function as $V(y) = py^2$. In the discrete-time case, p is a positive constant and $\mathrm{d}V(y)$ is the change in V between successive visits to the Poincaré section. In the continuous-time case, p is a positive function of the angle θ, $\mathrm{d}V(y)$ is the Lie derivative of $V(y)$ along the trajectories of the system (2). The quantity p is obtained by solving the corresponding Riccati equation. This equation is either associated with a second-order estimation of the Poincaré map (6) or the continuous flow (2). In the continuous-time case, we discretize the variable along the limit-cycle, and solve a family of sum-of-squares programs to generate the values of $p(\theta)$. The solution of

optimization problem (12) gives an inner estimation of the region of attraction as $\Omega_r = \{x \in T\mathscr{Q}_r : |y| < \frac{\sqrt{\rho}}{p}\}$.

3.5 Impact Map Analysis and Controller Improvements

The control laws studied so far perform reasonably well; however, the states typically jump away from the desired manifold $\mathscr{M} = \{\varphi - \varphi_{ref} = 0\}$ at the heelstrike. A considerable control effort must then be expended so that φ approaches φ_{ref} again. To remedy this situation, we analyze the impact map further to devise a family of methods to modify φ_{ref} in a desirable manner.

From the form of the impact map Ξ in equation (3), we observe that the post-impact torso velocity $\dot{\varphi}^+$ equals its pre-impact value, $\dot{\varphi}^-$, plus the term $\xi_2(\varphi)\dot{\theta}^-$. This suggests a robust method that precludes the impact event from disturbing the convergence $\varphi \to \varphi_{ref}$:

1. Find $\varphi^\star$ such that $\xi_2(\varphi^\star) = 0$, $\varphi^\star \in [\gamma, \frac{\pi}{2} + \gamma]$
2. Find the nominal limit cycle so that $\varphi_{ref} = \varphi^\star$,
3. Compute the transverse dynamics and the accompanying time-varying LQR closed-loop controller,
4. Have φ track φ_{ref} by using the control law (11).

In fact, we can take this observation one step further and find a family of methods that will perform favorably to a naïve nominal limit cycle selection. To that end, consider replacing point (1) above by the following steps:

(1a) Pick an function $f(\Xi)$ of the impact map to optimize, e.g., no change in post-impact torso velocity, least decrease in post-impact wheel velocity, etc.,
(1b) Perform the optimization to find the optimizer $\varphi^\star$.

The search for nominal limit cycle in step (2) may be conducted by using a nonlinear solver to find the fixed point of the Poincaré map $P(\cdot, \varphi^\star) : \mathbb{R} \to \mathbb{R}$. The values of the Poincaré map are obtained by numerically simulating the reduced system forward in time.

If the optimization problem in (1b) is unconstrained, then there may exist no nominal limit cycle for the output $\varphi^\star$ (i.e., the rimless wheel stumbles and falls back on the pre-impact stance spoke). In this case, the optimization can be repeated with an increased lower bound for φ until such a nominal limit cycle found. If any nominal limit cycle exists, this procedure will guarantee an optimal solution thanks to the following two propositions, which jointly show that increasing φ will increase the the walking speed $|\dot{\theta}|$ whenever the speed is small.

Proposition 1 *For the reduced system* (2)*, $\dot{\theta}$ is a decreasing function of φ for small $|\dot{\theta}|$ and $\gamma \le \varphi \le \frac{\pi}{2} + \gamma$.*

Proof. Straightforward calculation shows that

$$\frac{\mathrm{d}}{\mathrm{d}t}\frac{\partial}{\partial \dot{\theta}}\left(\frac{1}{2}\tilde{m}(q)\dot{\theta}^2\right) = \tilde{m}(q)\ddot{\theta} + \tilde{c}(q,\dot{\theta})\dot{\theta} = -\tilde{g}(q).$$

Integrating both sides over time yields

$$\begin{aligned}\tilde{m}(q(t))\dot{\theta}(t) = m_t g l_1 \int_0^t \sin(\theta(\sigma) - \gamma)\,\mathrm{d}\sigma \\ - m_2 g l_2 \int_0^t \sin(\varphi - \gamma)\,\mathrm{d}\sigma.\end{aligned}$$

Differentiating both sides with respect to φ we find

$$\frac{\partial \dot{\theta}}{\partial \varphi} = -\frac{m_2 l_2}{\tilde{m}(q)}\left(g\cos(\varphi - \gamma)t + l_1 \sin(\varphi - \theta)\dot{\theta}\right).$$

Since the coefficient on the right hand side is negative and the continuous flow takes a finite amount of time ($t > 0$), we deduce that $\dot{\theta}$ is a decreasing function of φ as long as $|\dot{\theta}|$ is bounded and small.

The above proposition makes sense as long as we can prove that $\dot{\theta}$ is bounded. This is true with a mild assumption on φ.

Proposition 2 *The speed $|\dot{\theta}|$ of the rimless wheel under the reduced model* (2) *is finite as long as $\varphi > \alpha$.*

Proof. Consider the Lyapunov function candidate

$$V(\theta, \dot{\theta}) = \frac{1}{2}\tilde{m}(q)\dot{\theta}^2 + m_t g l_1 (1 + \cos(\theta - \gamma)).$$

Taking the Lie derivative along the solutions of (2) and manipulating gives

$$\dot{V} = m_2 l_2 \dot{\theta}\left(\frac{l_1}{2}\sin(\varphi - \theta)\dot{\theta}^2 - g\sin(\varphi - \gamma)\right).$$

Assuming $\dot{\theta} < 0$, $\dot{V} < 0$ whenever $\frac{l_1}{2}\sin(\varphi - \theta)\dot{\theta}^2 \ge g\sin(\varphi - \gamma)$. For sufficiently large $|\dot{\theta}|$, this inequality is satisfied. Since the impact map Δ contracts $|\dot{\theta}|$ as well, we conclude that $|\dot{\theta}|$ is finite.

As an example of the above procedure, consider the problem of stabilizing a walking gait that requires the least energy to maintain. In the absence of friction, the system loses energy through the impact events. In particular, observe that $\Xi_2(q;\alpha) \to I$ as $\alpha \to 0$, which implies a continuum of spokes, i.e., a circular (rimmed) wheel. When $\alpha > 0$, on the other hand, it is always the case that $\mathscr{H}(q,\dot{q}) > \mathscr{H} \circ \Delta(q,\dot{q})$, where $\mathscr{H}$ denotes the total energy of the system. It follows that the closer Ξ_2 is to the identity

TABLE 1: Parameters of the system

(l_1, l_2) [m]	(m_1, m_2) [kg]	(I_1, I_2) [kg $\cdot$ m^2]
$(0.26, 0.05)$	$(2.32, 4.194)$	$(0.0784160, 0.0380256)$

map, the smaller is the energy loss of the walking gait. Therefore, we pose and solve the following following optimization problem to come up with a desired nominal torso angle

$$\begin{aligned} \underset{\varphi}{\text{minimize}} \quad & \|I - \Xi_2(\varphi)\|_F^2 \\ \text{subject to} \quad & \gamma < \varphi < \frac{\pi}{2} + \gamma, \end{aligned} \tag{13}$$

where $\|\cdot\|_F$ denotes the Frobenius norm of a matrix. For this particular system, this objective function can be expressed as $\|I - \Xi_2(\varphi)\|_F^2 = (1 - \xi_1(\varphi))^2 + \xi_2^2(\varphi)$.

Remark 1 *Note that Ξ_2 also depends on the inertial parameters and the link lengths. Although we do not pursue it here, one can also cast the energetically-optimal walking problem into a mechanism design problem. One would seek to choose the spoke length and the torso length such that $\|I - \Xi_2(\varphi)\|_F^2$ is uniformly minimized.*

Remark 2 *Extensive simulation studies show that even if the desired nominal gait is not selected such that the nominal torso reference angle equals $\varphi^\star$, where $\varphi^\star$ is the angle that minimizes energy loss at impact, it is energetically more efficient to smoothly deform the reference from φ_{ref} to $\varphi^\star$ as the walking gait nears heelstrike (use any smooth homotopy from the function $\varphi_{ref} : T\mathcal{Q} \to \mathbb{S}^1$ to the constant signal $\varphi^\star : T\mathcal{Q} \to *$).*

4 Simulation Studies

We present and compare simulation results for the controllers we discussed in the previous Section 3. The parameters we use for the simulations are selected to match an actual implementation of the robot and are summarized in Table 1.

4.1 Discrete-Time (DT) Controller

To derive the DT controller, we first obtain the approximation of the Poincaré map as described in Section 3.1. With the system parameters given in Table 1, the coefficients, α_η of the Poincaré map are presented in Table 2. We then find the nominal limit cycle by solving the optimization problem described in Section 3.5. The angular velocity of the wheel at $\theta = 0$ on the nominal limit cycle is computed to be $\dot{\theta}^\star = -0.65\,[\frac{\text{rad}}{\text{s}}]$. The corresponding nominal torso angle is $\varphi_0 = 18.26^\circ$.

For the computed nominal limit cycle, the linear portion of the estimated Poincaré map yields a DLQR controller gain of

TABLE 2: Coefficients of Poincaré map approximation

$\alpha_{0,0}$	$\alpha_{1,0}$	$\alpha_{0,1}$	$\alpha_{2,0}$	$\alpha_{0,2}$	$\alpha_{1,1}$
-0.842	0.498	-1.813	-0.0567	0.623	-0.183

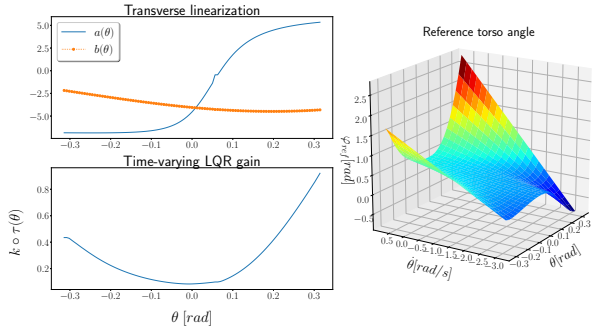

FIGURE 2: Transverse state and input functions $a(\theta)$, $b(\theta)$ the optimal control gain $k(\theta)$. The reference torso angle is computed by $\varphi_{ref} = \varphi_0 + k(\theta)(\dot{\theta} - \dot{\theta}^\star)$.

$K = -0.212\,[\text{s}]$. The reference torso angle each time the reduced system hits this section is given by $\varphi_{ref} = \varphi_0 + K(\dot{\theta} - \dot{\theta}^\star)$.

The torso position so generated is taken as a reference, which is asymptotically stabilized for the full system as described in Section 3.3. To generate the simulation results shown in Figure 3, we used the initial condition $x_{\text{initial}} = (\theta, \varphi, \dot{\theta}, \dot{\varphi}) = (0, \frac{\pi}{2} + \gamma, \frac{1}{2}, 0)$, where the wheel starts moving in the reverse direction. The response of the system under the DT controller is shown by the dotted, diamond, red curves.

4.2 Continuous-Time (CT) Controller

The implementation of CT controller parallels that of the DT controller. We still derive a nominal limit cycle but this time interpolate it as a function of time and subsequently the wheel angle θ. We use the same nominal limit cycle characterized by $\dot{\theta}^\star = -0.65\,[\frac{\text{rad}}{\text{s}}]$ at $\theta = 0$ with $\varphi_0 = 18.26^\circ$.

Using a numerical interpolation of the nominal limit cycle, we derive the transverse linearization, given by the functions $a(t)$ and $b(t)$ in equation (9). Figure 2 shows the transverse linearization, the time-varying LQR gain k and the corresponding reference torso angle φ_{ref}, expressed as functions of θ and $\dot{\theta}$.

The full system uses the inverse dynamics controller (Section 3.3) to exponentially steer φ to this φ_{ref}. For ease of comparison with the DT controller, we start the system at exactly the same initial condition even though the CT controller affords to be started at an even more adverse initial condition (such as a larger positive initial wheel velocity, see Section 4.3). The behavior of the full system dynamics under the CT controller is shown in Figure 3 as the solid, triangle, blue curves.

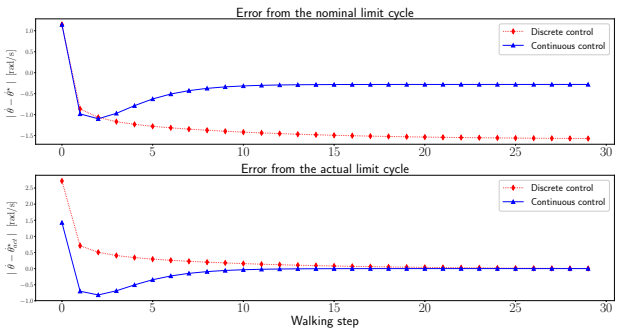

FIGURE 3: Convergence of the DT and CT controllers to the nominal and actual limit cycles.

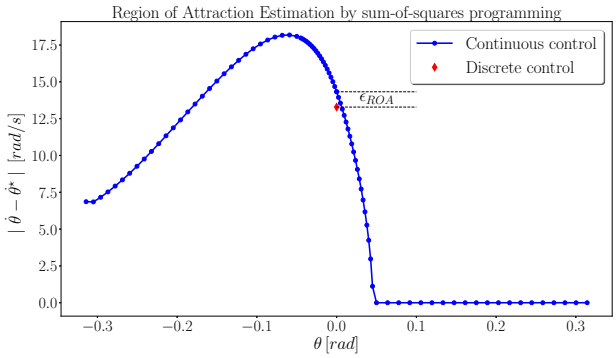

FIGURE 4: Regions of attraction of the DT and CT controllers, $\varepsilon_{ROA} = 1.038$ [rad/s].

We can use the CT controller to smoothly stabilize on terrains with varying slopes as well. The animation for such a simulation may be viewed at `https://youtu.be/mRcX6S_rvFE`.

4.3 Comparison of the CT and DT Controllers

The top plot in Figure 3 shows that the CT controller tracks the nominal limit cycle, derived from the reduced model, much more closely. The DT controller converges to a completely different limit cycle, that walks much faster, when applied to the full system.

The bottom plot in Figure 3 shows the transient response of the controllers as they converge to their respective walking gaits. We observe that the CT controller outperforms the DT controller with a faster convergence.

Figure 4 depicts the regions of attraction of the CT and DT controllers. The red diamond shows the estimated region of attraction of the DT controller, which is only computed at the Poincaré section characterized by $\theta = 0$. The region of attraction of the CT controller is given for various Poincaré sections, $-\alpha \leq \theta \leq \alpha$. We observe that on the section $\theta = 0$, the region of attraction of the CT controller is greater than that of the DT controller by an amount $\varepsilon_{ROA} = 1.038$ [rad/s]. We also observe that the region of attraction estimation correctly predicts that if the system is started with too great a wheel velocity in the opposite direction, the robot will stumble and fall back on its swing foot.

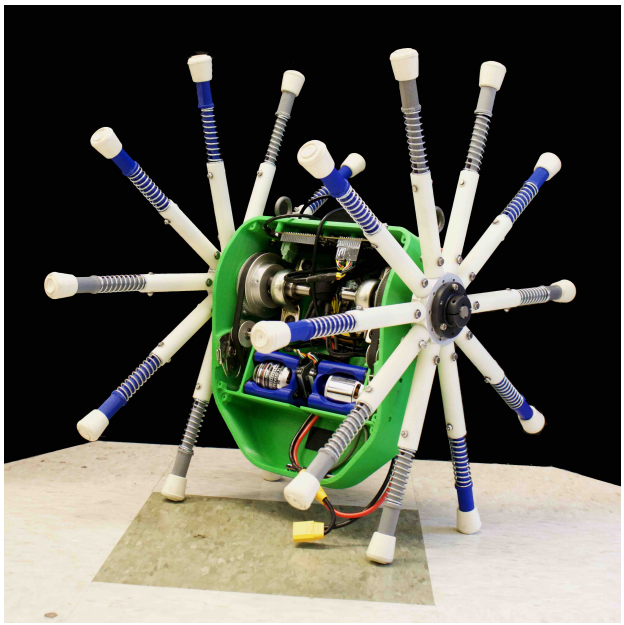

FIGURE 5: Experimental prototype

5 Experimental Studies

We describe how the implementation of the rimless wheel with torso and provide experimental results that support the theory developed earlier.

5.1 Prototype

Figure 5 shows the experimental prototype. It consists of two sets of rimless wheels, each with 10 spokes, attached side-to-side through a torso that houses all the electronics, motors, and batteries. The spokes and the torso are 3D printed using a hobby-grade printer (Makerbot replicator). Each spoke of the wheel has an inline compression spring to cushion the collision. Each rimless wheel is connected to an outrunner motor (Turnigy Aerodrive SK3 5055-280 KV, Hobbyking, Hong Kong) through a belt drive. Each motor has a capacitive encoder (AMT102 8192 counts per revolution, CUI Inc.,Tualatin, OR, USA) and controlled by an Odrive v3.5 motor controller (Odrive, CA, USA). The Odrive is connected to a Raspberry Pi 3B (Raspberry Pi foundation, UK). In addition, the torso is connected to a 9-axis inertial measurement unit (Adafruit, NY, USA). The motors are

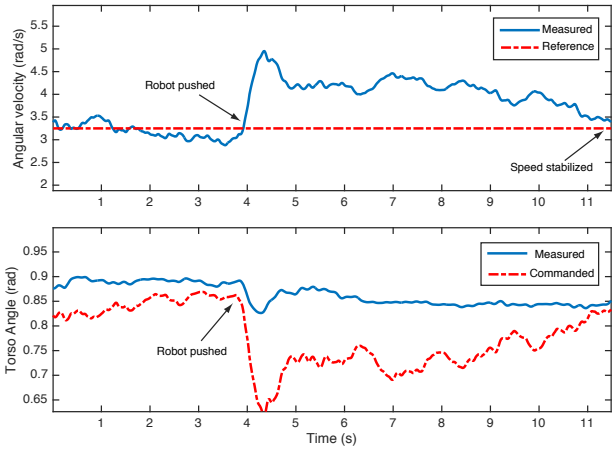

FIGURE 6: Experimental results

powered by a Turnigy 3000mAh 6S 30C Lipo Pack w/XT-60 and the electronics and computers are powered by Turnigy 1300mAh 6S 35C Lipo Pack.

5.2 Results

We implemented the continuous-time controller on the hardware with constant k gain. We chose a nominal torso angle of $\varphi_0 = 0.873\,[\text{rad}]$ (50°). This corresponds to a nominal linear hip speed of $0.8[\frac{\text{m}}{\text{s}}]$ or an angular speed of $\dot{\theta}^\star = 3.25[\frac{\text{m}}{\text{s}}]$ at $\theta = 0$. Figure 6 (a) shows the angular velocity of the stance leg ($\dot{\theta}$), and (b) shows torso angle (φ), both as a function of time. The robot is manually pushed at $t = 4$ sec, thus increasing its mid-stance speed to 5 rad/s. The controller compensates by reducing the torso angle. It takes the controller about 7 seconds or about 50 steps to get the system back to the nominal limit cycle, The slow response is because the proportional-integral-derivative controller for the torso is conservatively tuned and takes appreciable time to change the set-point.

6 Conclusion

We present a family of controllers for robustly stabilizing walking gaits of a rimless wheel with torso on various ground slopes. These controllers are derived by asymptotically stabilizing the transverse dynamics of the reduced system along a nominal limit cycle, judiciously selected to minimize the energy loss at impacts. Several other sensible choices for the nominal limit cycles exist, such as one for which the pre-impact and post-impact angular velocity of the torso coincide, etc. We support the theoretical development by numerical simulations and an eventual implementation on hardware.

REFERENCES

[1] McGeer, T., 1990. "Passive dynamic walking". *The International Journal of Robotics Research,* ***9***(2), pp. 62–82.

[2] Chatterjee, A., and Garcia, M., 2000. "Small slope implies low speed for mcgeer's passive walking machines". *Dynamics and Stability of Systems,* ***15***(2), pp. 139–157.

[3] Gomes, M., and Ruina, A., 2011. "Walking model with no energy cost". *Physical Review E,* ***83***(3), p. 032901.

[4] Jeans, J. B., and Hong, D., 2009. "Impass: Intelligent mobility platform with active spoke system". In Robotics and Automation, 2009. ICRA'09. IEEE International Conference on, IEEE, pp. 1605–1606.

[5] Asano, F., and Kawamoto, J., 2012. "Passive dynamic walking of viscoelastic-legged rimless wheel". In Robotics and Automation (ICRA), 2012 IEEE International Conference on, IEEE, pp. 2331–2336.

[6] Asano, F., Sogawa, T., Tamura, K., and Akutsu, Y., 2013. "Passive dynamic walking of rimless wheel with 2-dof wobbling mass". In Intelligent Robots and Systems (IROS), 2013 IEEE/RSJ International Conference on, IEEE, pp. 3120–3125.

[7] Asano, F., and Xiao, X., 2012. "Output deadbeat control approaches to fast convergent gait generation of underactuated spoked walker". In System Integration (SII), 2012 IEEE/SICE International Symposium on, IEEE, pp. 265–270.

[8] Bhounsule, P. A., Ameperosa, E., Miller, S., Seay, K., and Ulep, R., 2016. "Dead-beat control of walking for a torso-actuated rimless wheel using an event-based, discrete, linear controller". In Proc. 40th mechanisms and robotics conference, ASME.

[9] Henzinger, T. A., 2000. "The theory of hybrid automata". In *Verification of Digital and Hybrid Systems*. Springer, pp. 265–292.

[10] Goebel, R., Hespanha, J., Teel, A. R., Cai, C., and Sanfelice, R., 2004. "Hybrid systems: generalized solutions and robust stability". In Proc. 6th IFAC symposium in nonlinear control systems, Citeseer, pp. 1–12.

[11] Westervelt, E. R., Chevallereau, C., Choi, J. H., Morris, B., and Grizzle, J. W., 2007. *Feedback control of dynamic bipedal robot locomotion*. CRC press.

[12] Shiriaev, A. S., and Freidovich, L. B., 2009. "Transverse linearization for impulsive mechanical systems with one passive link". *IEEE Transactions on Automatic Control,* ***54***(12), pp. 2882–2888.

[13] Manchester, I. R., 2010. "Transverse dynamics and regions of stability for nonlinear hybrid limit cycles". *arXiv preprint arXiv:1010.2241*.

[14] Spong, M. W., 1994. "Partial feedback linearization of underactuated mechanical systems". In International Conference on Intelligent Robots and Systems (IROS), Vol. 1, IEEE, pp. 314–321.

[15] Khalil, H., 2002. *Nonlinear Systems*. Pearson Education. Prentice Hall.

[16] Tan, W., Packard, A., et al., 2008. "Stability region analysis using polynomial and composite polynomial lyapunov functions and sum-of-squares programming". *IEEE Transactions on Automatic Control,* ***53***(2), p. 565.